Quadratic superlattices: A type of nonperiodic lattice with extended states

D. S. Citrin*

School of Electrical and Computer Engineering, Georgia Institute of Technology, Atlanta, Georgia 30332-0250, USA

(Received 30 January 2023; accepted 16 March 2023; published 27 March 2023)

Deterministic nonperiodic lattices often exhibit properties intermediate between those of random and periodic crystals. Properties that have attracted interest include complex heirarchical structure factors, the breaking up of the band into a dense set of critical states and minigaps, and the interplay between extended and localized states. In one dimension, considerable attention has focused on nonperiodic lattices showing properties intermediate between periodic and random. We propose a one-dimensional nonperiodic lattice with lattice sites at 0^2d, 1^2d, 2^2d, ... with length d playing the rôle of the lattice constant. Here we show that the structure factor $S_0(k)$, which governs how waves are scattered and is reflected in many physical properties, is simply related to the Jacobi theta function $\vartheta_3(q)$. $S_0(k)$ is periodic in wave vector k and is singular continuous, consisting of a dense set of peaks with k given by rational-fraction multiples of $\frac{\pi}{d}$, though the scaling properties of $S_0(k)$ are the same as for periodic crystals. The electronic structure considered in a tight-binding model shows a bandlike spectrum, but broken by a dense set of minigaps near peak locations in $S_0(k)$. These lattices show novel properties such as the coexistence of a singular-continuous spectrum with extended states. Quadratic lattices may enable the physical realization of special functions of mathematical and physical importance as well as for the design of nonperiodic diffraction gratings, antenna arrays, ad coupled optical resonators to produce complex quasirandom behavior and are of interest to study quantum interactions in nonperiodic optical lattices.

DOI: 10.1103/PhysRevB.107.125150

I. INTRODUCTION

Periodic crystals, the stuff of textbook solid-state physics, have been under investigation for over a century. Periodic order leads to consequences that are familiar to any physics student, such as the Bloch theorem, delocalized states, and energy bands and bandgaps [1], and some that are not, such as the scaling behavior of the structure factor (SF) [2]. The presence of random disorder in crystals, which breaks strict periodicity, has also been studied for many years, and overall, the effect from a purely practical perspective is often to *degrade* the properties associated with the ideal periodic crystal [3].[1]

In the 1970's, the concept of a quasicrystal solidified [4–6]. A quasicrystal can be thought of as a nonperiodic tiling of the plane by a finite set of tiles. Quasicrystals can have rotational symmetries, but are not translationally invariant. While hints of the existence of quasicrystals in nature predated the first definitive reports, in 1984 Ref. [7] published results of the x-ray diffraction pattern from Al_6Mn and attributed anomalous features to the fact that the material is a quasicrystal. On the heels of this discovery, it was found that a one-dimensional chain of atoms spaced by a judiciously chosen Fibonacci sequence could be produced using a projection technique based on a two-dimensional periodic crystal yielding a one-dimensional quasicrystal [8]. Soon thereafter, Merlin *et al.* [9] realized that such a structure could be produced in a nonperiodic semiconductor superlattice (SL). This development also gave rise to explosive growth of interest in other types of nonperiodic, but deterministic, SLs, such as the Thue-Morse SL, though earlier interest in nonperiodic lattices can be found in Refs. [10–14]. More recently, there is interest in nonperiodic lattices in a range of systems [15], including interacting systems [16], nanosystems [17,18], and photonic systems [19]. Of special note, optical lattices are attracting attention [20–22].

One of the themes to emerge from such studies on nonperiodic lattices is that their physical properties may be intermediate between periodic and random [2,15]. While studies of various physical properties, including vibrational, electronic, and transport, of such nonperiodic SL ensued [15], a key quantity that often reveals the underlying structure in experiments is the SF. While the SF is typically directly related to the results of x-ray- and neutron-diffraction experiments, it also underlies behaviors observed in the vibrational, electronic, transport, and other properties.

In this contribution we report on theoretical work concerning a novel nonperiodic lattice we propose called a *quadratic chain* or *quadratic SL*. In this structure, the lattice sites are at positions $z = z_j$ with $z_j = j^2 d$, $j \in \mathbb{W}$ (whole numbers) as shown in Fig. 1. We show that the SF $S_0(k)$ has remarkable properties: (a) it is periodic in wave vector k with period $\frac{2\pi}{d}$; (b) $S_0(k)$ consists of a dense set of peaks with wave vectors $k_{r,s} = \frac{r}{s}\frac{\pi}{d}$ with r and s mutually prime integers with r and s of opposite parity; (c) the SF obeys a power law with respect to

*Also at Georgia Tech-CNRS IRL2958, Georgia Tech Europe, 2 Rue Marconi, 57070 Metz, France.

[1]Important and rich physics associated with disorder is related to localization effects that are qualitatively new behaviors not seen in the ordered crystal.

FIG. 1. Schematic diagram of the quadratic chain. $z_j = j^2 d$ labels positions of lattice sites (or atoms) (pink for $j = 0$, red for $j \in \mathbb{N}$) comprising the quadratic chain. The scattering amplitude of the sites in black is zero. The Fourier transform of this chain is the Jacobi theta function $\vartheta_3(q)$ with q the nome leading to a highly complex structure factor despite the quadratic chain's simplicity.

lattice length, i.e., $S_0(k_{r,s}) \propto L^{\gamma(k_{r,s})}$ with $L = N^2 d$ (with N the maximum value of j) the overall SL thickness and scaling parameter $\gamma(k_{r,s}) = 2$ as in the periodic and quasiperiodic cases; (d) the SF is straightforwardly expressed in terms of the Jacobi theta function $\vartheta_3(q)$ [23] and the spectrum exhibits properties of mathematical interest; that is, the quadratic SL enables the physical realization of a function of central importance; (e) the singular-continuous energy spectrum of the quadratic SL maintains an overall bandlike shape with the existence of extended (as well as localized) states for sufficiently weak on-site energies; the spectrum contains a dense set of energy eigenvalues and minigaps; (f) the quadratic lattice studied here is the simplest example of a class of lattices with z_j a polynomial in j with integer coefficients. In order to unveil the interesting behavior of the quadratic chain, we first compute the SF and then the electronic structure in a nearest-neighbor tight-binding model (NNTBM). While the quadratic chain shares certain characteristics of other celebrated nonperiodic lattices, such as Fibonacci and Thue-Morse, we shall see that several aspects of the quadratic chain stand out. These include (1) the relationship between the SF and the Jacobi theta function, (2) the full classification of the peaks in the SF which is distinct from that for other nonperiodic chains, and (3) the periodicity in wave vector of the SF.

II. STRUCTURE FACTOR

The SF gives the x-ray scattering strength in the first Born approximation, but also underlies numerous other physical properties such as the electronic structure in the perturbative limit, and it is thus to the SF that we first turn our attention. The quadratic chain is defined by function

$$p(z) = \sum_{j=0}^{\infty} \left(1 - \frac{1}{2}\delta_{0j}\right)\delta(z - z_j) \tag{1}$$

with positions $z_j = j^2 d$ of the lattice sites along the z axis and d a fundamental length. The fact that the lattice site z_0 receives apparent special treatment is a mathematical convenience, and does not affect the results for long chain length. To obtain convergent results, we need to consider *finite-length* chains. To do so, we impose a window $w(z)$ on $p(z)$ and consider the SF associated with $f_0(z) = w(z)p(z)$; we will make two choices for $w(z)$, viz., (i) $\Pi(2Nz/d + \frac{1}{2})$ with $N \in \mathbb{N}$ or (ii) $e^{-\alpha|z|}$ with $\alpha > 0, \alpha \in \mathbb{R}$. $\Pi(y)$ is the unit rectangle function with $\Pi(y) = 1$ for $y \in (-\frac{1}{2}, \frac{1}{2})$, $\frac{1}{2}$ for $y = \pm\frac{1}{2}$, and 0 otherwise. $N + 1$ gives the number of *atoms* with nonzero scattering amplitude (the pink and red atoms in Fig. 1) in the chain (including the pink zeroth atom), while α gives the attenuation of the scattering amplitude of the atoms as z increases. As we discuss in Appendix B, these two ways of considering what in essence is a finite chain are equivalent for our purposes as chain length becomes large, viz., $N \to \infty$ or $\alpha \to 0$. The purpose of the window is twofold. First, the direct computation of the SF of $p(z)$ indeed does not exist. This in and of itself need not be viewed as a problem as any real quadratic chain or SL would be of finite length. Second, by computing the SF of $f_0(z)$, namely the windowed quadratic chain $p(z)$, we can systematically study its scaling properties as the window size becomes large.

We now define the SF. We have $S_0(k) = |F_0(k)|^2$ with $F_0(k)$ the Fourier transform of $f_0(z)$ (the convention for the Fourier transform is in Appendix A). *Scaling* means the power-law behavior, alternatively (i) $L^{\gamma(k)} = (N^2 d)^{\gamma(k)} \propto S_0(k)$ for $L \to \infty$ for the finite-length chain (the conventional definition) or (ii) $\alpha^{-\gamma(k)} \propto S_0(k)$ for $\alpha \to 0$. Before moving on, we relate the number N of atoms in the quadratic chain (for N large, we can approximate $N + 1$ by N) to chain length $L = N^2 d$ in a finite-length quadratic chain and by extension to α in an infinite-length quadratic chain. For the quadratic chain $\alpha^{-1} \sim L = N^2 d$. In Appendix G we show

$$\gamma(k) \sim -\frac{1}{\ln N} \ln S_0(k) \sim -\frac{2}{\ln \alpha d} \ln S_0(k). \tag{2}$$

Note the factor of 2 in the numerator in the rightmost expression.

To compute $S_0(k)$, we focus here on the approach of case (ii) which more easily yields closed-form expressions. Substituting the expression for $f_0(t)$, we have $F_0(k) = \frac{1}{2}\vartheta_3(q)$ with $\vartheta_3(q)$ a Jacobi theta function

$$\vartheta_3(q) = 1 + 2\sum_{j=1}^{\infty} q^{j^2} \tag{3}$$

and $q = \exp[-i(k - i\alpha)d]$ the nome [24].[2] Consequently, the SF is simply $S_0(k) = \frac{1}{4}|\vartheta_3(q)|^2$. Inasmuch as $\vartheta_3(q)$ is a Fourier series in k, $S_0(k)$ is periodic in k with period $\frac{2\pi}{d}$. It is remarkable that the theta function arises straightforwardly from such a simple form for $p(z)$. $\vartheta_3(q)$ appears in such disparate fields as number theory, the solution to the heat-conduction equation, and in the study physical systems in multiply connected spaces [25]. As we shall see below, wave vectors $k = k_{r,s} = \frac{r}{s}\frac{\pi}{d}$ with $r \in \mathbb{Z}$ (integers) and $s \in \mathbb{N}$ (natural numbers) play a special role giving the locations of the minima and peaks of $S_0(k)$.

Figure 2 shows $S_0(k)$ for (i) $N = 10$ (solid black curve) and (ii) $\alpha d = 0.01$ (dashed blue curve) taking $d = 1$ for $k \in [0, \pi/d)$. For case (i), we replace the upper limit in the summation defining $\vartheta_3(q)$ by N and for the nome take $q = \exp(-ikd)$. [The results for other values of k outside the range shown follow from $S_0(k) = S_0(k + 2\pi/d)$ and $S_0(k) = S_0(-k)$.] Note that $\alpha = 0.01$ corresponds roughly to $N = 10$.

[2]There are several notations current for theta functions. Please note the definition above.

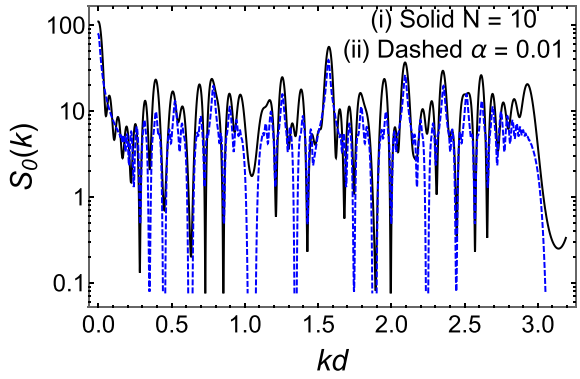

FIG. 2. $S_0(k)$ with $\alpha d = 0.01$ on a logarithmic scale. $S_0(k)$ is periodic with period $2\pi/d$. Also, $S_0(k) = S_0(-k)$; hence, we only show the SF within $k \in [0, \pi/d)$. Note that $\alpha = 0.01$ corresponds roughly to $N = 10$ (taking $d = 1$).

Indeed, the two curves are overall similar, though the dashed curve exhibits somewhat sharper peaks and troughs. The SF is composed of a complex sequence of peaks separated by minima, the positions of which are discussed below. As N increases or α decreases, the number of visually evident peaks increases and the peaks become sharper.

In Appendix E we discuss finding the locations of the zeros and the locations and magnitudes of the peaks in $S_0(k)$. The zeros (in the $N \to \infty$ or $\alpha \to 0$ limit) occur for r and s odd, viz., at wave vectors $k_{2m-1,2n-1} = \frac{2m-1}{2n-1}\frac{\pi}{d}$ with $m \in \mathbb{Z}$ and $n \in \mathbb{N}$. That is, for rational numbers with odd numerator and denominator. One easily verifies these wave vectors as the locations of the minima in Fig. 2.

We now turn our attention to the peaks in $S_0(k)$. The maxima occur at the two remaining classes of $k_{r,s} = \frac{r}{s}\frac{\pi}{d}$,with r and s of opposite parity, viz., $k_{2m,2n-1} = \frac{2m}{2n-1}\frac{\pi}{d}$ and $k_{2m-1,2n} = \frac{2m-1}{2n}\frac{\pi}{d}$. For $k_{2m,2n} = \frac{2m}{2n}\frac{\pi}{d}$, $2m$ and $2n$ are not mutually prime, and thus $k_{2m,2n}$ can be reduced to one of the above cases. The maxima seen in Fig. 2 are at the values of k just mentioned.

Next, we consider the scaling of the peaks in $S_0(k)$. For $k_{\xi,\eta}$ corresponding to a peak in $S_0(k)$, using method (i), we have for large N,

$$N^{\gamma(k_{r,s})} \sim S_0(k_{r,s}) \sim \left|\sum_{j=1}^{N} e^{-ik_{r,s}dj^2}\right|^2 \sim \frac{N^2}{\eta^2}\left|\sum_{j=1}^{\eta} e^{-ik_{r,s}dj^2}\right|^2, \tag{4}$$

noting that $e^{ik_{r,s}d}$ is an ηth root of unity for the appropriate $\eta \in \mathbb{N}$ (see Appendices E and F), whence $\gamma(k_{r,s}) = 2$, as for a periodic or quasiperiodic chain. The summations in the expression above are known as Gauss sums; closed-form expressions are given in Appendix F. The fact that $\gamma(k_{r,s}) = 2$ suggests that the corresponding electronic states can be *extended*. We shall later more carefully address the problem of extended states in the electronic structure. In Fibonacci chains, by contrast, the SF is composed of a dense set of peaks, but states exist that are critical—neither extended nor localized [15].

Using the results above, we can verify that the peak heights and positions are as expected. In Fig. 3 is shown $S_0(k)$ for $\alpha d = 0.001$ [case (ii)], identifying the positions and heights

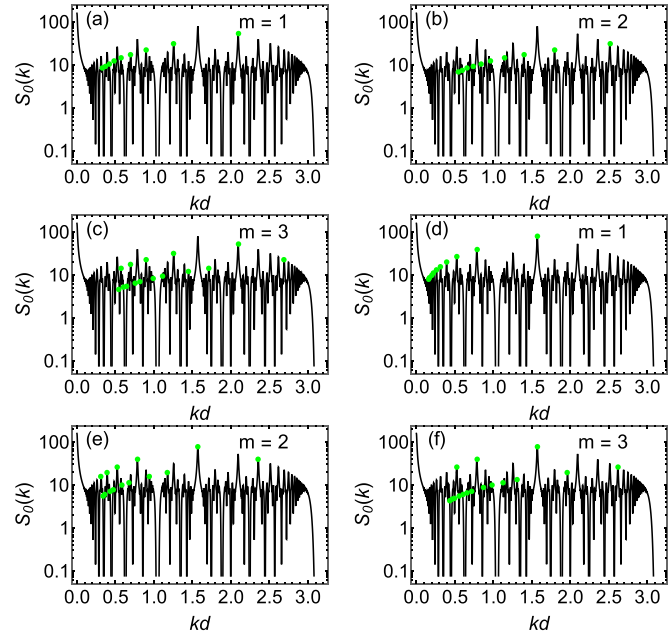

FIG. 3. $S_0(\omega)$ with $\alpha d = 0.001$ on a logarithmic scale. (a)–(c) shows the peak positions and heights (green dots) for $k_{2m,2n-1}$, while (d)–(f) for $k_{2m-1,2n}$. Note that some peaks are repeated as in these cases the relevant fraction $\frac{2m}{2n-1}$ or $\frac{2m-1}{2n}$ can be reduced to give a result found for a smaller value of m.

of selected peaks (green dots). In Figs. 3(a)–3(c) are shown the expected peak positions and heights for $k_{2m,2n-1}$, while Figs. 3(d)–3(f) for $k_{2m-1,2n}$. Note that some peaks are repeated as in these cases the relevant fraction $\frac{2m}{2n-1}$ or $\frac{2m-1}{2n}$ can be reduced to give a result found for a smaller value of m. In passing, note that case (ii) gives a closer visual representation to $S_0(k)$ for the infinite chain than case (i) for modest values of N.

We can see heuristically why $k_{r,s}$ with r and s of opposite parity determines the peaks. $S_0(k)$ peaks for wave vectors k such that the interferences between scattering from the various atoms is net constructive, i.e., after considering interference terms from all such scatterings. Nonetheless, for scattering between any pair of sites j and j' separated by an odd number $j - j'$, there is always an integer n such that $k_{2m-1,2n}(j^2 - j'^2)d$ is a multiple of 2π, while for $j - j'$ even, there is always an integer n such that $k_{2m,2n-1}(j^2 - j'^2)d$ is a multiple of 2π.

To close this section, we have found the SF $S_0(k)$ and its scaling behavior in closed form. $S_0(k)$ is singular continuous in the $N \to \infty$ or $\alpha \to 0$ limit and consists of a dense set of peaks given by ratios of mutually prime integers ξ and η multiplied by $\frac{\pi}{d}$ with ξ and η of opposite parity. The scaling parameter $\gamma(k_{r,s}) = 2$ in all cases as in a periodic or quasiperiodic chain. The appearance of $S_0(k)$ is complex; however, the peaks occur in families whose spacing and heights follow simple rules, as seen above in Fig. 3. Thus, the quadratic SL provides a route to physically realize $\vartheta_3(k)$ via $S_0(k)$.

III. ELECTRONIC STRUCTURE

The SF is of direct interest to describe physical phenomena in which the first Born approximation is valid. Nonetheless,

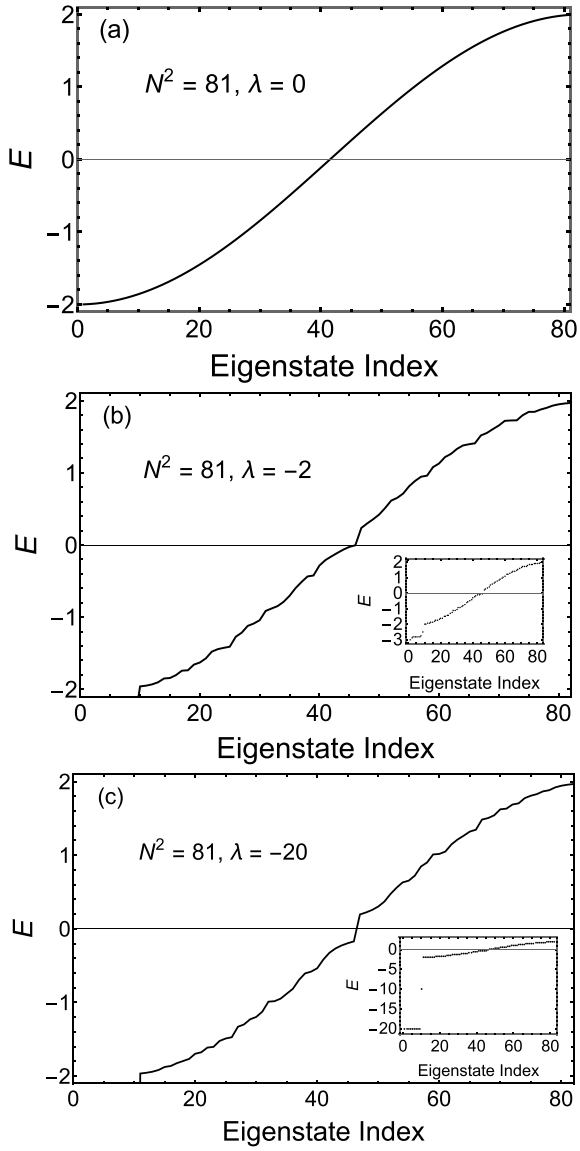

FIG. 4. Energy eigenvalues E of the nearest-neighbor tight-binding Hamiltonian $\hat{H}$ for an $N^2 = 81$ chain with (a) $\lambda = 0$, (b) -2, and (c) -20. The main frame restricts the energy scale to the spectra of the bandlike states, while the insets show the entire spectra including states strongly localized about $j^2 d$. We note an overall bandlike shape with strongly localized states at low energy. The spectrum exhibits a set of minigaps (see Fig. 5) closely correlated in position and magnitude with those in $S_0(k)$.

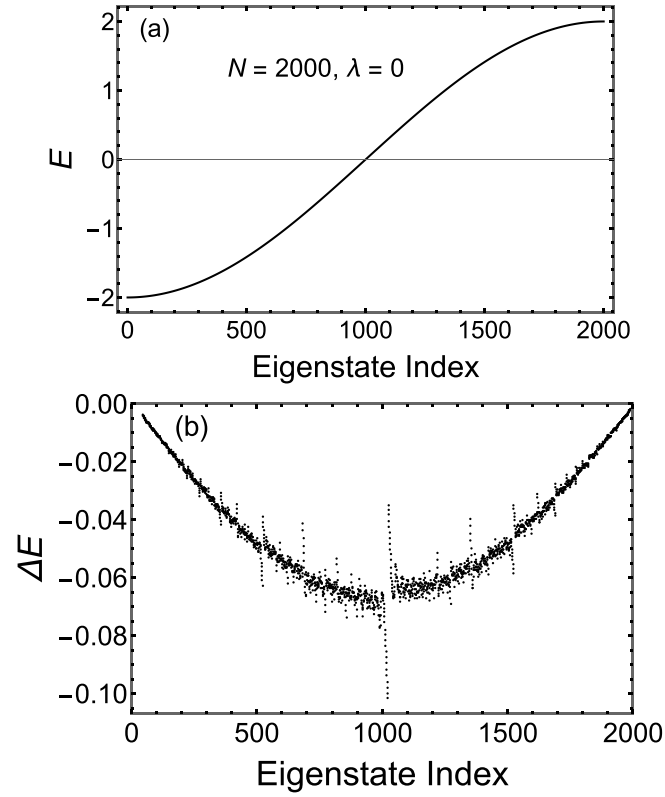

FIG. 5. (a) The energy eigenvalues E for for an $N^2 = 2000$ chain with $\lambda = -20$. The range on the vertical scale is limited so that the states localized about the sites $j^2 d$ do not appear. The minigaps are the small variations about the expected $-\cos kd$ band shape for $\lambda = 0$. (b) The difference ΔE between E for $\lambda = -20$ and 0 for $N^2 = 2000$. Compare with Fig. 2 aligning the horizontal axes. We observe a dense set of minigaps of magnitude correlated with the peaks in $S_0(k)$. The largest minigap occurs for an eigenstate index close to $N/2$, which in the case of $\lambda = 0$ is for $k \approx \frac{\pi}{2d}$.

it is known for various nonperiodic lattices that the SF often provides insight into a range of physical properties—not just into x-ray and neutron diffraction—that require description beyond the first Born approximation. We therefore consider the electronic structure of the quadratic chain in a simple NNTBM. The quadratic modulation is applied to the diagonal matrix elements in a fashion seen below corresponding to Fig. 1. We assume the following Hamiltonian $\hat{H}$ in the basis of atomic orbitals:

$$\hat{H}_{n,n'} = -\delta_{n,n'+1} - \delta_{n,n'-1} + \lambda\delta_{n,n'}\left(\delta_{n,\text{perfect square}} - \tfrac{1}{2}\delta_{n,0}\right), \quad n, n' \in \{0, N^2\}. \tag{5}$$

The subscripts n and n' here to refer to tight-binding sites n, while the label j is reserved to describe values of $n, n' = j^2$, i.e., the atoms in the quadratic chain when n is a perfect square. In other words, the interatomic matrix element between neighboring sites is -1, while the on-site potential is zero unless the site index is a perfect square in which case it is λ (or $\frac{\lambda}{2}$ for the zeroth site). The maximum value of n is chosen to be N^2.

As noted in Ref. [26], in the small-λ limit, perturbation theory–to the extent it may be valid as it relates the energy eigenvalue to $|V(k)|$ where potential $v(z)$ is due to the quadratic modulation with $V(k)$ the Fourier transform of $v(z)$, which closely resembles $F_0(k)$. For our problem, this means that peaks in $|F_0(k)|$ will manifest themselves in states and minigaps modifying the otherwise bandlike $E_0(k)$. As Cheng *et al.* argue for a Thue-Morse chain, one finds that even in the large-λ limit, minigaps are expected to open in the spectrum that are closely correlated with the features in the SF. In a similar fashion, as we show below, when λ is no longer small enough for perturbation theory to apply, indeed when all the states are expected to be localized, the spectrum still exhibits

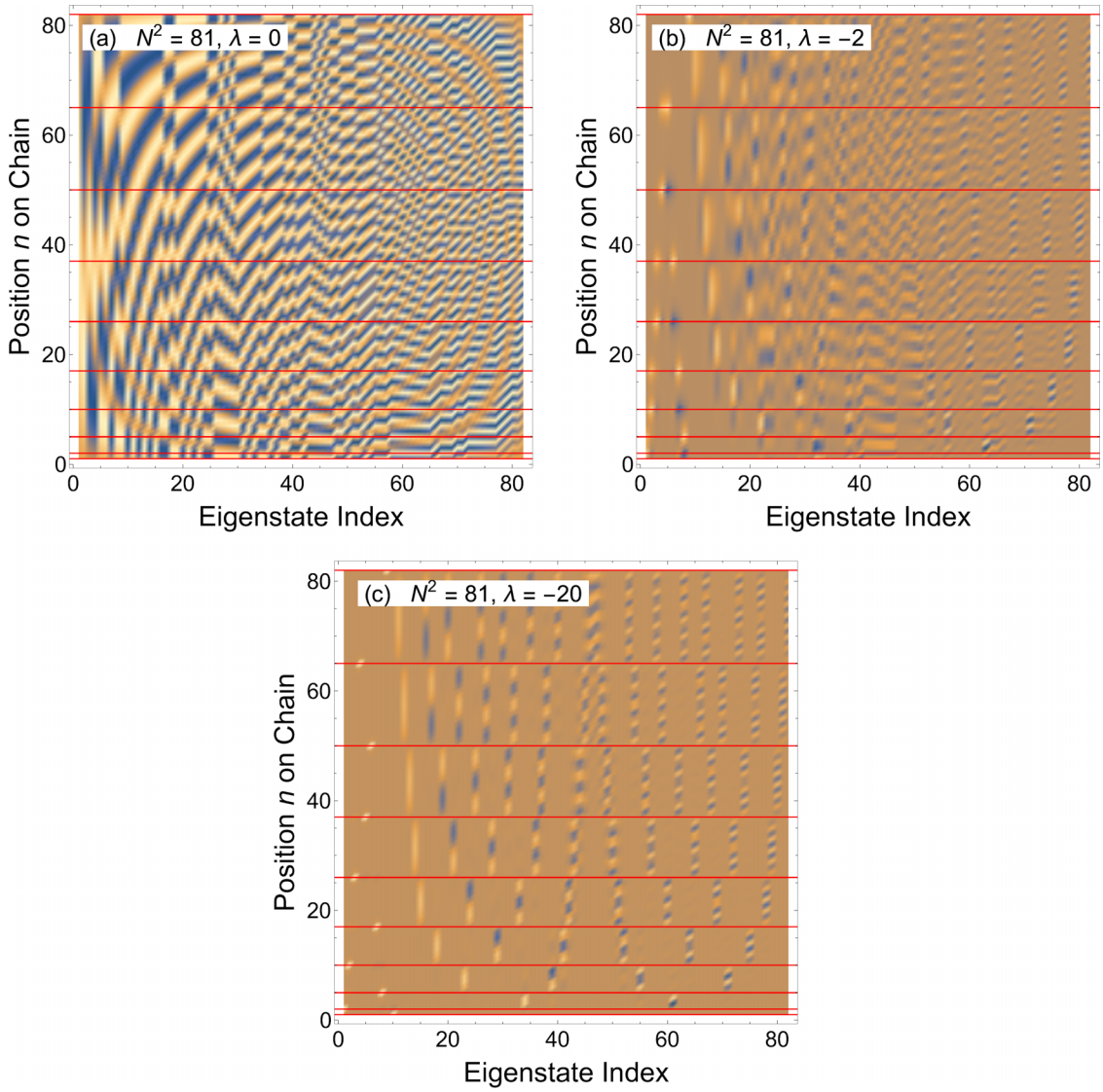

FIG. 6. Eigenstates for an $N^2 = 81$ chain with (a) $\lambda = 0$, (b) -2, and (c) -20. The color scale indicates higher probability density with brighter color. Horizontal bars are drawn at values of lattice sites n equal to a perfect square j^2. (a) The quadratic potential is absent. (b) Here the value of λ is in the regime beyond which perturbation theory fails. (c) This is the large-$|\lambda|$ regime.

a structure resembling $F_0(k)$ and may contain numerous extended states.

In Fig. 4 are plotted the eigenvalues E of $\hat{H}$ (roughly speaking the horizontal axis corresponds to kd and we thus employ that labeling) for an $N^2 = 81$ (chosen to illustrate the structure of the eigenstates) chain with (a) $\lambda = 0$, (b) -1, and (c) -20. The main frame restricts the energy scale to the spectra of the bandlike states, while the insets show the entire spectra including states strongly localized about $j^2 d$ at low energy, as can also be seen below in Fig. 6. The spectra exhibit an overall bandlike shape with strongly localized states around a given site at low energy lying below the bandlike states by $\sim\lambda$. The number of such states is N. The bandlike portion of the spectra exhibits minigaps (see Fig. 5) closely correlated in position and magnitude with features in $S_0(k)$. The minigaps size increases with $|\lambda|$. It should be noted that even in the case of $|\lambda|$ much greater than the halfwidth 2 of the band $E_0(k) = -2\cos kd$, and where all states are localized, the structures in the spectrum still reflect $S_0(k)$ while the overall shape continues to resemble $E_0(k)$. This shall be discussed further.

Figure 5 shows the difference between the results for $\lambda = 0$ and -20 for $N^2 = 2000$, here chosen large enough to reveal the rich structure. Aligning the horizontal scale from 0 to 2000 in Fig. 5 with the scale for kd in Fig. 2, we notice that the features in both plots are correlated in terms of position and relative amplitude. That is minigaps lie between peaks in $S_0(k)$ and the magnitudes of these minigaps are correlated with the peak heights in Fig. 2. Because $S_0(k)$ has peaks at all $k_{\xi,\eta} = \frac{\xi}{\eta}$ with ξ and η of opposite parity, these minigaps are dense as seen in Fig. 5.

Figure 6 shows the eigenstates of $\hat{H}$ for an $N^2 = 81$ chain with (a) $\lambda = 0$, (b) -2, and (c) -20. On the vertical axis are the positions n of the sites on the chain, while the horizontal

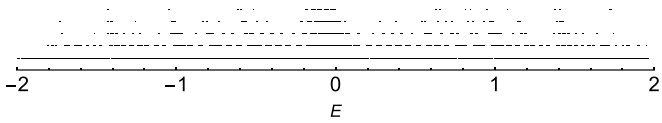

FIG. 7. Energies of extended states for $N^2 = 81$. From bottom to top: $\lambda = -0.1, -0.5, -1, -1.5, -2$. As $|\lambda|$ increases, there is an increasing tendency for states to be localized.

axis indexes the eigenstate in the same order at in Fig. 4. The colorscale indicates higher probability density with brighter color. Horizontal bars are drawn at values of lattice sites n equal to a perfect square j^2. Thus, for a given eigenstate, one reads up the plot to find the associated amplitude of the corresponding eigenstate on site n. In (a) the quadratic potential is absent. The states are simply the eigenfunctions of $\hat{H}$ for a uniform finite-length chain. (b) Here the value of λ is in the regime beyond which perturbation theory fails. We see toward the left-hand side low-energy states localized about individual sites in the quadratic chain; at higher energy are states that are more delocalized. (c) This is the large-$|\lambda|$ regime. We again see the states localized at individual quadratic sites at low energy. At higher energy, the states are localized within the various effective quantum wells between $n = j^2$ and $(j+1)^2$. The number of nodes for states confined between vertical bars at successive values of $n = j^2$ increases with eigenstate index. For a given number of nodes, states confined between successively smaller values of $n = j^2$ are at higher eigenstate index. Near eigenstate index $\frac{N^2}{2}$, specifically at 46 and 47, the largest minigap occurs, corresponding to the large feature in $S_0(k)$ at $kd = \frac{\pi}{2}$ as in Fig. 2.

We have also studied the states in the NNTBM via a transfer-matrix approach. In Fig. 7 we show the energies of extended states in an $N^2 = 81$ quadratic chain with $\lambda = -0.1$, -0.5, -1, -1.5, and -2. The extended states correspond to those for which eigenvalues of the transfer matrix lie on the unit circle in the complex plane (see Appendix H). The extended-state minibands break up as $|\lambda|$ increases with an increasing number of minigaps opening between the extended states. As $|\lambda| \gtrsim 2$, the extended states become too fragmentary to see on the plot and eventually all states become localized.

IV. CONCLUSION

We introduce the quadratic superlattice in which the positions of the atoms are $z_j = j^2 d$. The SF is found to be proportional to the square modulus of the Jacobi theta function $\vartheta_3(q)$ approaching the unit circle. Wave vectors $k_{r,s} = \frac{r}{s}\frac{\pi}{d}$ play a special role in the SF. For r and s both odd, $k_{r,s}$ is a zero of the SF. For r and s of opposite parity, $k_{r,s}$ corresponds to a maximum of the SF. The visual appearance of the SF is complex and is periodic in wave vector with period $\frac{2\pi}{d}$. The SF shows a scaling parameter $\gamma(k_{r,s}) = 2$, which is also the value found for periodic and quasiperiodic crystals. This value of the scaling factor indicates extended states; this is corroborated by results based on the NNTBM provided the on-site matrix element on the quadratic chain is sufficiently small.

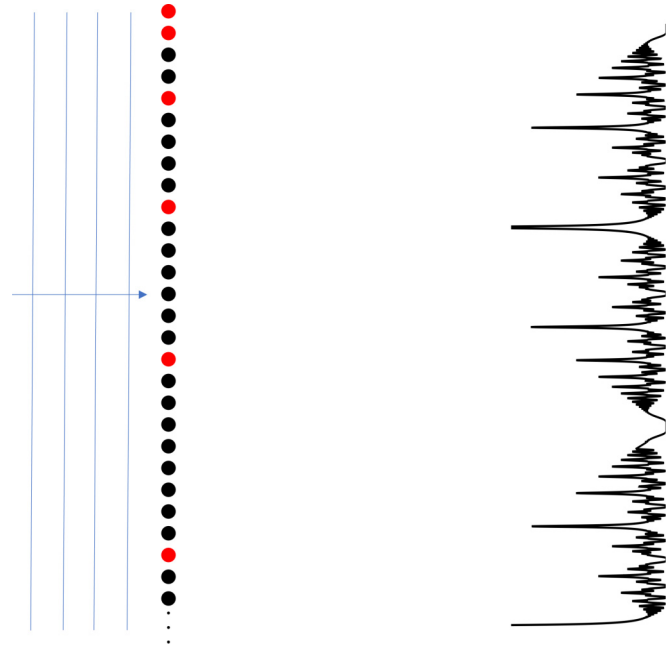

FIG. 8. Schematic diagram showing Fraunhofer diffraction from a quadratic grating. Plane-wave light at normal incidence from the left. The intensity diffraction pattern appearing on a screen is shown to the right. More than one period is shown.

While the SF is of direct relevance to x-ray and neutron diffraction, it also plays an outsized role in various physical properties. We therefore numerically study the electronic structure of a quadratic chain in a NNTBM where the quadratic structure is in the on-site matrix elements. While perturbation theory shows that in the weak-modulation limit, the lowest-order correction to the energy directly reflects the features of $S_0(k)$, the SF also manifests its features well outside the range of validity of perturbation theory. The quadratic modulation opens a dense set of minigaps in the otherwise bandlike spectrum where the size and positions of the minigaps are between the peaks in the SF.

Nonperiodic chains have already been proposed to enable the physical realization of functions of importance to to mathematics [27]; here we see that the quadratic chain leads to the Jacobi zeta function $\vartheta_3(q)$. From a broader perspective, the quadratic chain is just the simplest of a class of nonperiodic lattices in which $z_j = \sum_{\nu=0}^{t} \beta_\nu j^\nu$ with integer coefficients β_ν. Further generalizations might involve multidimensional theta functions [28] to account for nonperiodic lattices in more than one dimension. On a different note, gratings and antenna arrays following a quadratic sequence are of potential interest to produce complex, including quasirandom, diffraction patterns or radiation patterns that are nonetheless deterministic. In the Fraunhofer approximation, as in Fig. 8, the diffraction or radiation patterns are given directly by $S_0(k)$; however, in the Fresnel approximation, the relationship is not so close, but one expects complex behavior. (Meeting the Fraunhofer approximation will require large distances or relatively small N.) Unlike Fibonacci and Thue-Morse chains, the quadratic chain has a SF whose maxima have scaling properties similar to those of periodic crystals. In addition, $S_0(k)$ for the quadratic

chain qualitatively exhibits complexity while resulting from a deterministic structure. We might add that quadratic chains may be realized in various physical systems, including in optical lattices of cold atoms and in magnetic systems, providing rich future opportunities for study.

ACKNOWLEDGMENTS

D.S.C. gratefully acknowledges the support of Conseil Régional Grand Est and CPER SusChemProc.

APPENDIX A: DEFINITIONS

As in the main text, we consider the distribution

$$p(z) = \sum_{j=0}^{\infty} \left(1 - \frac{1}{2}\delta_{0j}\right)\delta(z - z_j) \tag{A1}$$

giving the positions z_j with $z_j = j^2 d$. Note that we can equivalently take $p(z) = \frac{1}{2}\sum_{j=-\infty}^{\infty}\delta(z - z_j)$. We impose a window $w(z)$ on $p(z)$ and consider $f_0(z) = w(z)p(z)$; $w(z)$ will be chosen to be (i) $\Pi(2Nz/d + \frac{1}{2})$ with $N \in \mathbb{Z}^+$ or (ii) $e^{-\alpha|z|}$ with $\alpha > 0$ real. Here, $\Pi(y) = 1$ for $y \in (-\frac{1}{2}, \frac{1}{2})$, $\frac{1}{2}$ for $y = \pm\frac{1}{2}$, and 0 otherwise is the unit rectangle function. The factor $e^{-\alpha|z|}$ describes a spatially decreasing scattering amplitude with increasing z.

As a preliminary, we define the SF $S_0(k)$. $S_0(k)$ is the modulus square of the Fourier transform $F_0(k)$ of $f_0(z)$ with k the wave vector. In general, the Fourier transform $G(k)$ of function $g(z)$ (in the distribution sense) and the associated inverse Fourier transform (provided they exist) are

$$G(k) = \int_{-\infty}^{\infty} dz\, g(z)e^{-ikz}, \tag{A2a}$$

$$g(z) = \frac{1}{2\pi}\int_{-\infty}^{\infty} dk\, G(k)e^{ikz}. \tag{A2b}$$

Specifically, the SF of $f_0(z)$ is then

$$S_0(k) = |F_0(k)|^2, \tag{A3}$$

i.e., the power spectrum of $f_0(z)$.

APPENDIX B: WINDOW FUNCTION $w(z)$

That (i) and (ii) provide alternatives to understand the long-length behavior of a chain is due to the fact that in the spectral domain, the product $f_0(z) = w(z)p(z)$ assumes the form of a convolution $F_0(k) = W(k) * P(k)$. For cases (i) and (ii), $W(k)$ has similar properties in the large-N and small-α limits.

1. Case (i)

Here, $w(z) = \Pi(2Nz/d)$. The Fourier transform $W(k)$ of $w(z)$ is

$$W(k) = \frac{2\sin kN/d}{k}.$$

Noting that $(\sin \pi x)/(\pi x)$ is the normalized sinc function, we see that the integral over k of $W(z)$ is 2π. At $k = 0$ we have

$$W(0) = 2Nd.$$

2. Case (ii)

Here, $w(z) = e^{-\alpha|z|}$. The Fourier transform $W(k)$ of $w(z)$ is

$$W(k) = 2\pi\frac{\alpha/\pi}{k^2 + \alpha^2}.$$

The factor $\frac{\alpha}{\pi}/(k^2 + \alpha^2)$ is the normalized Lorentzian (Cauchy) distribution. Thus, the integral over k of $W(z)$ is 2π. At $k = 0$ we have

$$W(0) = \frac{2}{\alpha}.$$

Comparing cases (i) and (ii), we see that in both cases first that $W(k)$ integrates to 2π regardless of the value of the respective parameter N or α and second that (i) $W(0) = 2Nd$ or (ii) $W(0) = 2/\alpha$. This suggests that the large-N limit of (i) and the small-α limit of (ii) provide similar information on the scaling properties of $S_0(k)$.

APPENDIX C: DIGRESSION ON THE PERIODIC CHAIN

To discuss the SF, we begin with a digression on semi-infinite periodic chains and provide a concrete comparison of (i) and (ii), viz. $p(z) = \sum_{j=1}^{\infty}\delta(z - z_j)$ with $z_j = jd$, so that

$$f_0(z) = \sum_{j=1}^{N}\delta(z - z_j), \quad \text{case(i)}, \tag{C1a}$$

$$f_0(z) = \sum_{j=1}^{\infty}\delta(z - z_j)e^{-\alpha z}, \quad \text{case(ii)}. \tag{C1b}$$

For the periodic chain, it is well known [2] for (i) that $\gamma(0) = 2$ with $S_0(k \neq 0) = 0$ in $k \in [0, \pi/d)$. [We only consider $k \in [0, \pi/d)$ as $S(k) = S(k + 2\pi/d)$ and $S(k) = S(-k)$.] Now, let us consider procedure (ii). A direct calculation gives of Eq. (C1b) gives

$$S_0(0) = \frac{1}{e^{2\alpha d} - 2e^{\alpha d} + 1}. \tag{C2}$$

In the limit $\alpha \to 0$, we have, expanding the exponentials in the denominator to lowest nonvanishing order in αd,

$$S_0(0) = \frac{1}{(\alpha d)^2}. \tag{C3}$$

Thus, $-\ln S_0(0)/\ln \alpha d \sim 2$ for small α. Thus we compute identical $\gamma(k)$ based on either the window functions of (i) and (ii).

APPENDIX D: THE QUADRATIC CHAIN

Figure 2 shows $S_0(k)$ on a logarithmic scale with (i) $N = 10$ (solid black curve) and (ii) $\alpha d = 0.01$ (dashed blue curve) taking for simplicity (and without loss of generality) $d = 1$ plotted for $k \in [0, \pi/d)$. For case (i), we replace the upper limit in the summation in Eq. (3) by N and for the nome take $q = \exp(-ikd)$. Note that $\alpha = 0.01$ corresponds roughly to $N = 10$. The SF is composed of a complex sequence of peaks separated by minima, the positions of which are discussed below. As N increase or α decreases, the number of peaks visually evident increases. Apart from minor differences, such

as the peaks and troughs for case (II) are sharper than for case (i), the two curves are quite similar.

APPENDIX E: ZEROS AND MAXIMA OF $S_0(k)$

We shall find the zeros and maxima of $S_0(k)$ using methods (i) and (ii), and see in both cases that the results may be expressed in terms of Gauss sums. $S_0(k)$ will be found to diverge at its peaks in the $N \to \infty$ or $\alpha \to 0$ limit, a direct consequence of the fact that the unit circle in q is the natural boundary of the region of analyticity of $\vartheta_3(q)$.

1. Method (i)

The $N \to \infty$ limit of $S_0(k)$ is determined by

$$M = \lim_{N\to\infty}\left(1 + 2\sum_{j=1}^{N}\bar{q}^{j^2}\right) \sim 2\lim_{N\to\infty}\sum_{j=1}^{N}\bar{q}^{j^2}, \tag{E1}$$

where $\bar{q} = e^{ikd}$. This sum is only defined when $k = k_{2\xi,\eta} = \frac{2\xi}{\eta}\frac{\pi}{d}$ with $\xi, \eta \in \mathbb{Z}$ in that limit. We shall only be interested in values of $\eta \in \mathbb{N}$. Note that for $k = k_{2\xi,\eta}$, q is a ηth root of unity. Thus,

$$M \sim 2\left\lfloor \frac{N}{\eta} \right\rfloor \sum_{j=1}^{\eta}\bar{q}^{j^2} + 2\sum_{j=\lfloor N/\eta\rfloor+1}^{N}\bar{q}^{j^2} \sim 2\frac{N}{\eta}\, g(\xi;\eta) \tag{E2}$$

with

$$g(\xi;\eta) = \sum_{j=1}^{\eta} e^{ik_{2\xi,\eta}dj^2} = \sum_{j=1}^{\eta} e^{2\pi i\frac{\xi}{\eta}j^2} \tag{E3}$$

a Gauss sum to be evaluated below.

2. Method (ii)

We now explore the asymptotic behavior of $\vartheta_3(q)$ on the unit circle. Write $q = \bar{q}e^{-\alpha d}$ where $\bar{q}$ is an ηth root of unity, viz., $\bar{q} = e^{ik_{2\xi,\eta}d}$. We have

$$\begin{aligned}
\vartheta_3(\bar{q}e^{-\alpha d}) &= 1 + 2\sum_{j=1}^{\infty} e^{-\alpha d j^2}\bar{q}^{j^2} \\
&= 1 + 2\left[\sum_{j=1}^{\eta} e^{-\alpha d j^2}\bar{q}^{j^2} + \sum_{j=\eta+1}^{2\eta} e^{-\alpha d j^2}\bar{q}^{j^2}\right. \\
&\quad \left. + \sum_{j=2\eta+1}^{3\eta} e^{-\alpha d j^2}\bar{q}^{j^2} + \cdots\right] \\
&= 1 + 2\left[\sum_{j=1}^{\eta} e^{-\alpha d j^2}\bar{q}^{j^2} + \sum_{j=1}^{\eta} e^{-\alpha d (j+\eta)^2}\bar{q}^{j^2}\right. \\
&\quad \left. + \sum_{j=1}^{\eta} e^{-\alpha d (j+2\eta)^2}\bar{q}^{j^2} + \cdots\right] \\
&= 1 + 2\sum_{j=1}^{\eta}\bar{q}^{j^2}\sum_{\nu=0}^{\infty} e^{-\alpha d\eta^2(\nu+j/\eta)^2}.
\end{aligned} \tag{E4}$$

We can find the following bounds on $\sum_{\nu=0}^{\infty} e^{-\alpha d\tilde{n}^2(\nu+j/\eta)^2}$ by approximating as an integral,

$$\begin{aligned}
\sum_{\nu=0}^{\infty} e^{-\alpha d\eta^2(\nu+j/\eta)^2} &\geqslant \int_0^{\infty} d\nu\; e^{-\alpha d\eta^2(\nu+j/\eta)^2} \\
&= \frac{1}{2\eta}\sqrt{\frac{\pi}{\alpha d}}\,\mathrm{erfc}\left(\frac{j}{\eta}\sqrt{\alpha}\right), \\
\sum_{\nu=0}^{\infty} e^{-\alpha d\eta^2(\nu+j/\eta)^2} &\leqslant \int_0^{\infty} d\nu\; e^{-\alpha d\eta^2(\nu-1+j/\eta)^2} \\
&= \frac{1}{2\eta}\sqrt{\frac{\pi}{\alpha d}}\,\mathrm{erfc}\left[\left(\frac{j}{\eta}-1\right)\sqrt{\alpha}\right],
\end{aligned}$$

where

$$\begin{aligned}
\frac{1}{2\eta}\sqrt{\frac{\pi}{\alpha d}}\,\mathrm{erfc}\left[\left(\frac{j}{\eta}-1\right)\sqrt{\alpha}\right] &\leqslant \sum_{\nu=0}^{\infty} e^{-\alpha d\eta^2(\nu+j/\eta)^2} \\
&\leqslant \frac{1}{2\eta}\sqrt{\frac{\pi}{\alpha d}}\,\mathrm{erfc}\left(\frac{j}{\eta}\sqrt{\alpha}\right).
\end{aligned} \tag{E5}$$

Inasmuch as $\frac{1}{\eta} \leqslant \frac{j}{\eta} \leqslant 1$, as $\alpha \to 0$, we obtain the asymptotic expression

$$\sum_{\nu=0}^{\infty} e^{-\alpha d\eta^2(\nu+j/\eta)^2} \sim \frac{1}{2\eta}\sqrt{\frac{\pi}{\alpha d}}. \tag{E6}$$

Therefore, returning to Eq. (E4), we have (see Ref. [29], p. 79 noting the prefactor of 2 in front of the summation in Eq. (E4))

$$\vartheta_3(\bar{q}e^{-\alpha d}) \sim \frac{1}{\eta}\sqrt{\frac{\pi}{\alpha d}}\sum_{j=1}^{\eta}\bar{q}^{j^2} = \frac{1}{\eta}\sqrt{\frac{\pi}{\alpha d}}\, g(\xi;\eta), \tag{E7}$$

expressing the asymptotic form of $\vartheta_3(\bar{q}e^{-\alpha d})$ as $\alpha \to 0$ in terms of a Gauss sum.

APPENDIX F: EVALUATION OF THE GAUSS SUM $g(\xi;\eta)$

We present closed-form expressions of the Gauss sum $g(\xi;\eta)$. We employ Theorems 1.5.1, 1.5.2, and 1.5.3 of Ref. [30]. Let $\xi \in \mathbb{Z}$ and $\eta \in \mathbb{N}$ with ξ and η mutually prime. Then,

$$g(\xi;\eta) = \begin{cases} \left(\frac{\eta}{\xi}\right)(1+i)^{\xi}\sqrt{\eta}, & \eta \equiv 0 \mod 4, \\ 0, & \eta \equiv 2 \mod 4, \\ \left(\frac{\xi}{\eta}\right)\sqrt{\eta}, & \eta \equiv 1 \mod 4, \\ \left(\frac{\xi}{\eta}\right)i\sqrt{\eta}, & \eta \equiv 3 \mod 4, \end{cases} \tag{F1}$$

where $\left(\frac{\xi}{\eta}\right)$ denotes the Jacobi symbol [31]. In the order of the cases considered in Eq. (F1), we have

$$k_{2\xi,\eta} = \begin{cases} \frac{\xi}{\eta/2}\frac{\pi}{d}, & \xi \text{ odd}, \eta/2 \text{ even}, \\ \frac{\xi}{\eta/2}\frac{\pi}{d}, & \xi \text{ odd}, \eta/2 \text{ odd}, \\ \frac{2\xi}{\eta}\frac{\pi}{d}, & 2\xi \text{ even}, \eta \text{ odd}, \\ \frac{2\xi}{\eta}\frac{\pi}{d}, & 2\xi \text{ even}, \eta \text{ odd}. \end{cases} \tag{F2}$$

Thus, for the four cases, k is a rational multiple of $\frac{\pi}{d}$. In the main paper, we use the following notation for the cases in Eq. (F2):

$$k_{2\xi,\eta} = \begin{cases} k_{2m-1,2n} &= \frac{2m-1}{2n}\frac{\pi}{d}, \quad \text{maximum}, \\ k_{2m-1,2n-1} &= \frac{2m-1}{2n-1}\frac{\pi}{d}, \quad \text{zero}, \\ k_{2m,2n-1} &= \frac{2m}{2n-1}\frac{\pi}{d}, \quad \text{maximum}, \\ k_{2m,2n-1} &= \frac{2m}{2n-1}\frac{\pi}{d}, \quad \text{maximum} \end{cases} \tag{F3}$$

for the appropriate m and n where the rightmost label classifies the wave vector as corresponding to a maximum or zero of $S_0(k)$. Note that the two subscripts of k are mutually prime. Thus, the maxima are at wave vectors that are rational fractions times $\frac{\pi}{d}$ with the numerator and denominator of opposite parity while for the zeros, the numerator and denominator are both odd. (If the numerator and denominator are both even, they cannot be mutually prime.)

Figure 3 of the main paper shows that these limiting expressions well predict the peak heights and positions in $S_0(k)$.

APPENDIX G: SCALING PROPERTIES OF THE MAXIMA OF $S_0(k)$

The scaling properties of the SF $S_0(k)$ (assuming power-law behavior) in method (ii) are given by

$$\begin{aligned}\gamma(k_{\xi,\eta}) &= -\frac{2}{\ln \alpha d}\ln S_0(k) \\ &= -\frac{2}{\ln \alpha d}\left[-\ln \alpha d + \ln\left(\frac{\pi}{4\eta^2}\left|\sum_{j=1}^{\eta}\bar{q}^{j^2}\right|^2\right)\right] \sim 2.\end{aligned} \tag{G1}$$

Therefore, the peaks of the SF all obey power-law scaling with an exponent $\gamma(k) = 2$, as in periodic and quasiperiodic crystals.

By the way, we can arrive at the comparable result using method (i). For large N, consider

$$F_0(k_{2\xi,\eta}) \sim \sum_{j=1}^{N}\bar{q}^{j^2}. \tag{G2}$$

Thus,

$$F_0(k_{2\xi,\eta}) \sim \frac{N}{\eta}\sum_{j=1}^{\eta}\bar{q}^{j^2},$$

giving $\gamma(k_{2\xi,\eta}) = 2$.

1. The case $k = 0$

We separately consider the scaling of the peaks in $S_0(k)$ as $\alpha \to 0$ dispensing at the same time with the trivial set of wave vectors $k_{2\xi,1} = 2\pi\xi/d$. We focus on $k_{0,1} = 0$, the results for which also hold for $k_{2\xi,1}$. Using procedure (i), we have for large N for $k_{0,1}$,

$$N^{\gamma(0)} \sim S_0(0) = |F_0(0)|^2 \sim N^2, \tag{G3}$$

where $\gamma(0) = 2$, as in the case of a periodic chain as seen above.

We next corroborate this result against procedure (ii), the $\alpha \to 0$ limit for the infinite chain. One has for the asymptotic behavior of $\vartheta_3(q)$ as $\alpha \to 0$ for $k_{0,1}$, $\vartheta_3(q) \sim \sqrt{\pi/(\alpha d)}$ [32], where

$$S_0(0) \sim \frac{\pi}{4\alpha d} \tag{G4}$$

and

$$\begin{aligned}\gamma(0) &= -\frac{2}{\ln\alpha}\ln S_0(0) \sim -\frac{2}{\ln\alpha}\ln\frac{\pi}{4\alpha d} \\ &= -\frac{2}{\ln\alpha}(\ln\pi - 2\ln 2 - \ln\alpha d) \sim 2.\end{aligned} \tag{G5}$$

Again, methods (i) and (ii) provide identical scaling properties of $S_0(k)$.

APPENDIX H: NEAREST-NEIGHBOR TIGHT-BINDING MODEL

In the main text we present numerical results from a NNTBM for finite quadratic chains. The Hamiltonian is

$$\begin{aligned}\hat{H}_{n,n'} = &-\delta_{n,n'+1} - \delta_{n,n'-1} + \lambda\delta_{n,n'}\left(\delta_{n,\text{perfect square}} - \tfrac{1}{2}\delta_{n,0}\right), \\ &n, n' \in \{0, N\}.\end{aligned} \tag{H1}$$

The subscripts n and n' here to refer to tight-binding sites n, while subscript j is reserved for values of $n, n' = j^2$, i.e., when n is a perfect square. We use a transfer-matrix approach discussed in Ref. [33]. We can write the time-independent Schrödinger equation as

$$\begin{pmatrix}\psi_{n+1}\\ \psi_n\end{pmatrix} = M_n\begin{pmatrix}\psi_n\\ \psi_{n-1}\end{pmatrix} \tag{H2}$$

relating the amplitudes ψ_{n-1}, ψ_n, and ψ_{n+1} on sites $n-1$, n, and $n+1$, where M_n is the transfer matrix

$$M_n = \begin{pmatrix}-(E-\lambda_n) & -1\\ 1 & 0\end{pmatrix} \tag{H3}$$

with $\lambda_n = \lambda$ if $n = j^2$ is a perfect square (other than 0), $\frac{\lambda}{2}$ if $n = 0$, and 0 otherwise. We can thus take M_0 to be the matrix with $\lambda_n = \lambda_0 = \frac{\lambda}{2}$, M_1 to be the matrix with $\lambda_n = \lambda_1 = \lambda$, and M_2 to be the matrix with $\lambda_n = \lambda_2 = 0$ for $n > 0$. By iterating, we obtain

$$\begin{pmatrix}\psi_{(j+1)^2}\\ \psi_{(j+1)^2-1}\end{pmatrix} = \prod_{m=1}^{j}\left[M_2^{2(j-m+1)}M_1\right]\begin{pmatrix}\psi_1\\ \psi_0\end{pmatrix}. \tag{H4}$$

Inasmuch as M_2 is unimodular, we have via a special case of the Cayley-Hamilton theorem [33–35]

$$M_2^{2j} = U_{2j-1}(x)M_2 - U_{2j-2}(x)I, \tag{H5}$$

where $U_v(x)$ is a Chebyshev polynomial of the second kind and $x = \frac{1}{2}\text{Tr}M_2 = -\frac{E}{2}$. In order to find candidate extended states, we need to look within the bandwidth $|E| < 2$ determined by the interatomic matrix element between neighboring sites which is 1. $U_v(x)$ accounts for this as it blows up rapidly for $|x|$ increasing above 1. Note that

$$\left|\det\prod_{j=m}^{j}\left[M_2^{2(j-m+1)}M_1\right]\right| = 1. \tag{H6}$$

The eigenvalues of

$$\prod_{m=1}^{j}\left[U_{2(j-m)+1}\left(\tfrac{E}{2}\right)M_2 - U_{2(j-m)}\left(\tfrac{E}{2}\right)I\right]M_1 \tag{H7}$$

on the unit circle in the complex plane give the energies E for the extended states of the system as in Fig. 7 of the main text.

1. The limit $\lambda \to \pm\infty$

We now consider the large-$|\lambda|$ limit. Here, all states are strongly localized. For the case $\lambda \to \pm\infty$, there will be states closely localized at $n = j^2$ as seen in Fig. 6 of the main text; there will also be states localized between $n = j^2$ and $(j+1)^2$ whose wave functions' amplitude will vanish on $n = j^2$ and $(j+1)^2$. We have

$$\begin{pmatrix}\psi_{(j+1)^2}\\ \psi_{(j+1)^2-1}\end{pmatrix} = M_2^{2j}\begin{pmatrix}\psi_{j^2+1}\\ \psi_{j^2}\end{pmatrix}, \tag{H8}$$

where

$$\begin{pmatrix}\psi_{(j+1)^2}\\ \psi_{(j+1)^2-1}\end{pmatrix} = \begin{pmatrix}0\\ \pm 1\end{pmatrix}, \quad \begin{pmatrix}\psi_{j^2+1}\\ \psi_{j^2}\end{pmatrix} = \begin{pmatrix}1\\ 0\end{pmatrix}. \tag{H9}$$

Using Eqs. (H3), (H5), and (H9) in Eq. (H8), we have the simultaneous equations

$$\begin{aligned} 2xU_{2j-1}(x) - U_{2j-2}(x) &= 0\\ U_{2j-1}(x) &= \pm 1. \end{aligned} \tag{H10}$$

In fact, the solutions to the first of Eq. (H10) are a subset of the second. Once the solutions x are found, we obtain the energy eigenvalues for these states via $x = -\frac{E}{2}$.

Let us now find these solutions x. For a given value of j, there are $2j$ solutions. Let us begin with the first of Eq. (H10). Note that the Chebyshev polynomial of the second kind is defined as

$$U_n(\cos\theta) = \frac{\sin(n+1)\theta}{\sin\theta}. \tag{H11}$$

It is easily shown that the solutions of the first of Eq. (H10) are

$$x = \cos\tfrac{m\pi}{2j+1} \tag{H12}$$

with $m = 1, 2, 3, \cdots, 2j$. We have for the left-hand side of the first of Eq. (H10) substituting in Eq. (H12),

$$\cos\tfrac{m\pi}{2j+1}\ \frac{\sin\frac{2jm\pi}{2j+1}}{\sin\frac{m\pi}{2j+1}} - \frac{\sin\frac{(2j-1)m\pi}{2j+1}}{\sin\frac{m\pi}{2j+1}}, \tag{H13}$$

which is easily shown to vanish using elementary trigonometric identities.

We note that the solutions x are exactly what is expected based on quite elementary considerations. Consider the effective quantum well confined between infinite potentials at $n = j^2$ and $(j+1)^2$. This quantum well is thus of width $2j+1$. The zero boundary conditions at j and $(j+1)^2$ give standing-wave solutions with wave vectors $k_{m,2j+1} = \frac{m\pi}{2j+1}$ with $m = 1, 2, 3, \cdots, 2j$. (The quantum-well mode for $2j+1$ at the Brillouin-zone boundary results in zero amplitude on each lattice site, and must therefore be discounted here.) The $2j$ wave vectors $k_{m,2j+1}$ give energies $E = E_{m,2j+1} = -2\cos k_{m,2j+1}$ which are precisely the solutions of the first of Eq. (H10) given in Eq. (H12).

Notice the resemblance between the zeros of the Chebyshev polynomial of the first kind [36] and Fig. 6(c) of the main text. The values of x in Eq. (H12) are the extrema of $T_{2j+1}(x)$. The main point is that between each pair of sites j^2 and $(j+1)^2$ are the expected quantum-well states.

[1] F. Bloch, Über die quantenmechanik der elektronen in kristallgittern, Z. Phys. **52**, 555 (1929).

[2] R. Merlin, Structural and electronic properties of nonperiodic superlattices, IEEE J. Quantum Electron. **24**, 1791 (1988).

[3] A. Guinier, *X-Ray Diffraction in Crystals, Imperfect Crystals, and Amorphous Bodies* (W. H. Freeman, San Francisco, 1963).

[4] H. Wang, Toward mechanical mathematics, IBM J. Res. Develop. **4**, 2 (1960).

[5] R. Penrose, The role of aesthetics in pure and applied mathematical research, Bull. Inst. Math. Appl. **10**, 266 (1974).

[6] A. L. Mackay, Crystallography and the Penrose pattern, Physica A **114**, 609 (1982).

[7] D. Shechtman, I. Blech, D. Gratias, and J. W. Cahn, Metallic Phase with Long-Range Orientational Order and No Translational Symmetry, Phys. Rev. Lett. **53**, 1951 (1984).

[8] R. K. P. Zia and W. J. Dallas, A simple derivation of quasicrystalline spectra, J. Phys. A **18**, L341 (1985).

[9] R. Merlin, K. Bajema, R. Clarke, F.-Y. Juang, and P. K. Bhattacharya, Quasiperiodic GaAs-AlAs Heterostructures, Phys. Rev. Lett. **55**, 1768 (1985).

[10] M. Y. Azbel, Quantum Particle in One-Dimensional Potentials with Incommensurate Periods, Phys. Rev. Lett. **43**, 1954 (1979).

[11] J. B. Sokoloff, Band structure and localization in incommensurate lattice potentials, Phys. Rev. B **23**, 6422 (1981).

[12] K. S. Dy and T. C. Ma, Electronic states in a one-dimensional system with incommensurate lattice potentials, J. Phys. C **15**, 6971 (1982).

[13] M. Kohmoto, L. P. Kadanoff, and C. Tang, Localization Problem in One Dimension: Mapping and Escape, Phys. Rev. Lett. **50**, 1870 (1983).

[14] T. Nagatani, Electronic states in one-dimensional self-similar alloy with (3^1, 3^2,..., 3^N) periods, Phys. Rev. B **30**, 6241 (1984).

[15] A. Jagannathan, The Fibonacci quasicrystal: Case study of hidden dimensions and multifractality, Rev. Mod. Phys. **93**, 045001 (2021).

[16] V. Brajuskovic, F. Barrows, C. Phatak, and A. K. Petford-Long, Real-space observation of magnetic excitations and avalanche behavior in artificial quasicrystal lattices, Sci. Rep. **6**, 34384 (2016).

[17] S. Kasture, A. P. Ravishankar, V. J. Yallapragada, R. Patil, N. V. Valappil, G. Mulay, and V. G. Achanta, Plasmonic quasicrystals with broadband transmission enhancement, Sci. Rep. **4**, 5257 (2014).

[18] D. V. Talapin, E. V. Shevchenko, M. I. Bodnarchuk, X. Ye, J. Chen, and C. B. Murray, Quasicrystalline order in self-

assembled binary nanoparticle superlattices, Nature (London) **461**, 964 (2009).

[19] Z. Vardeny, A. Nahata, and A. Agrawal, Optics of photonic quasicrystals, Nat. Photon. **7**, 177 (2013).

[20] M. M. Burns, J.-M. Fournier, and J. A. Golovchenko Optical matter: Crystallization and binding in intense optical fields, Science **249**, 749 (1990).

[21] L. Fallani, J. E. Lye, V. Guarrera, C. Fort, and M. Inguscio, Ultracold Atoms in a Disordered Crystal of Light: Towards a Bose Glass, Phys. Rev. Lett. **98**, 130404 (2007).

[22] K. Singh, K. Saha, S. A. Parameswaran, and D. M. Weld, Fibonacci optical lattices for tunable quantum quasicrystals, Phys. Rev. A **92**, 063426 (2015).

[23] R. Bellman, *A Brief Introduction to Theta Functions* (Holt, Rinehart, and Winston, New York, 1961).

[24] I. S. Gradshteyn and I. M. Ryzhik, *Tables of Integrals, Series, and Products* (Academic, New York, 2007), formula 8.180.4, trivially adapting the notation to emphasize the dependence on the nome taking $u = 0$ in the notation of this reference.

[25] See Chapter 23 of L. S. Schulman, *Techniques and Applications of Path Integration* (Dover, Mineola, NY, 2005).

[26] Z. Cheng, R. Savit, and R. Merlin, Structure and electronic properties of Thue-Morse lattices, Phys. Rev. B **37**, 4375 (1988).

[27] D. S. Citrin, Physical Realization of the Riemann Zeta Function: The Effects of Noise (unpublished).

[28] B. Deconinck, Chapter 21 Multidimensional Theta Functions, in *NIST Digital Library of Mathematical Functions*, Release 1.1.8 of 2022-12-15, edited by F. W. J. Olver, A. B. Olde Daalhuis, D. W. Lozier, B. I. Schneider, R. F. Boisvert, C. W. Clark, B. R. Miller, B. V. Saunders, H. S. Cohl *et al.*, https://dlmf.nist.gov/21 (2023)

[29] B. Moore, Theta Functions, Gauss Sums, and Modular Forms, Ph.D. Thesis, The University of Adelaide, 2020, https://digital.library.adelaide.edu.au/dspace/bitstream/2440/125691/1/Moore2020_MPhil.pdf.

[30] B. C. Berndt, R. J. Evans, and K. S. Williams, *Gauss and Jacobi Sums* (Wiley, New York, 1998).

[31] C. G. J. Jacobi, Über die Kreisteilung und ihre Anwendung auf die Zahlentheorie, J. für die reine und angewandte Mathematik **30**, 166 (1846).

[32] X. S. Wang, Asymptotics of the q-theta function, Commun. Math. Anal. **7**, 50 (2009).

[33] A. Chakrabarti, S. N. Karmakar, and R. K. Moitra, Role of a New Type of Correlated Disorder in Extended Electronic States in the Thue-Morse Lattice, Phys. Rev. Lett. **74**, 1403 (1995).

[34] A. Cayley, II. A memoir on the theory of matrices, Philos. Trans. R. Soc. London **148**, 17 (1958).

[35] F. Abeles, Annal. Phys. (Paris) **12**, 706 (1950).

[36] Zeros of the first 50 Chebyshev polynomials of the first kind, https://en.wikipedia.org/wiki/Chebyshev_nodes#/media/File:Chebyshev_Zeros.svg.